Plasmonic Interactions and Optical Forces between Au Bipyramidal Nanoparticle Dimers†

Rene A. Nome,‡ Mason J. Guffey,§ Norbert F. Scherer,‡,§ and Stephen K. Gray*,∥

Center for Nanoscale Materials, Argonne National Laboratory, Argonne, Illinois 60439, Department of Chemistry, 929 East 57th Street, The James Franck Institute, The University of Chicago, Chicago, Illinois 60637, Chemical Sciences and Engineering Division, Argonne National Laboratory, Argonne, Illinois 60439

Received: December 15, 2008

Interparticle forces that can be driven by applied (optical) fields could lead to the formation of new particle arrangements when assembled in arrays. Furthermore, the potentially large interactions and large local fields associated with plasmon excitations in anisotropic nanoparticles can lead to enhanced nonlinear responses and applications for sensing. These and other applications would benefit from simulations of spectra and forces arising from plasmonic interactions. We present the results of rigorous three-dimensional, finite-difference, time-domain calculations of near- and far-field properties of pairs of Au bipyramidal nanoparticles in three different configurations: side-by-side, head-to-tail, and face-on. The absorption and scattering spectra depend strongly on the geometry as well as on the interparticle separation, as intuitively expected from a dipole coupling picture. Bipyramidal dimers in head-to-tail and face-on geometries exhibit an increasingly red-shifted (longitudinal) plasmon resonance with decreasing separation, whereas side-by-side dimers exhibit a blue shift. Large resonant field enhancements at the gap between particles in a head-to-tail configuration indicate the strong coupling of plasmonic modes. The Maxwell stress tensor formalism is employed to calculate the optical force one particle exerts on the other. Both significant attraction and weak repulsion can be obtained, depending on the relative arrangement of the particles. The force between bipyramids in the head-to-tail configuration can be greater than 10 times the force between pairs of Au nanospheres with the same volume. Experimental linear scattering spectra of particles trapped using the plasmon-resonance-based optical trapping method are found to be consistent with two particles trapped in the side-by-side configuration.

1. Introduction

Creating materials with specific or enhanced function(s) typically relies on achieving ordered structures. These structures may, for example, allow obtaining a more uniform (homogeneous) response to a signal (e.g., electro-optic switching) or enhancement of response to a perturbation (e.g., sensing). Conversely, disordered materials may have "diffuse" electrical or optical responses.[1] Nanomaterials have the potential to enhance various functional properties by quantum confinement effects or local field enhancements. Self-assembly methods are typically used for ordering nanomaterials into 1-, 2- or 3-D structures. However, the structures achieved are often close packed[2] and represent the thermodynamically minimum energy state. The addition of auxiliary fields or potentials allows for the possibility of achieving new structures and, hence, materials with enhanced or even new functions.

Electromagnetic radiation in the visible range can induce surface charge density oscillations, termed surface plasmons (SPs), in metallic nanostructures.[3] Excitation of SPs gives rise to enhanced fields in close proximity to the nanoparticle surface. The large field gradients generated upon optical excitation of surface plasmons are expected to exert forces on polarizable objects. Experimental and theoretical studies of the optical properties of particle dimers are providing insights on plasmonic interactions between metallic nanoparticles.[4−7] These studies typically describe spectra and near-field properties of dimers excited with visible light. For incident field polarization orthogonal to the interparticle symmetry axis, the spectral properties of the dimer are weakly dependent on particle separation, resembling those of isolated particles except for a small blue shift of the dimer resonance. On the other hand, when the incident field polarization is oriented parallel to the interparticle axis, dipolar single-particle resonances red-shift as the interparticle separation decreases.

A complementary perspective is provided by the distance dependence of the SP-induced electric (near-) field distributions. At large separations relative to the size of the particles, the electric field near each particle shows a dipole-like pattern, with intense field distributions along the interparticle axis.[4] Furthermore, a strong field-enhancement at the gap between nanoparticles is observed as the separation decreases. Interparticle currents have been observed for separations smaller than ∼1 nm; these currents decrease the local field below that calculated by classical electrodynamics.[8,9]

The manipulation of microscopic objects using optical tweezers is based on light-induced forces that originate from large intensity gradients.[10] Recently, the electric-field gradients associated with strongly interacting plasmonic systems have been explored for the design of novel optical trapping technologies.[11−17] The resulting optical forces can be most rigorously calculated by integrating the Maxwell stress tensor (MST) over an appropriate surface and require knowledge of the total electromagnetic field for the system. For systems with dimensions much smaller than the wavelength of the incident field, the MST formalism yields gradient forces and radiation pressure.[18] Recent theoretical work on optical forces between

† Part of the "George C. Schatz Festschrift".

* To whom correspondence should be addressed. E-mail: gray@tcg.anl.gov.
‡ Center for Nanoscale Materials, Argonne National Laboratory.
§ The University of Chicago.
∥ Chemical Sciences and Engineering Division, Argonne National Laboratory.

10.1021/jp811068j CCC: $40.75
Published on Web 03/06/2009

metallic particles[19−25] typically employs spatially uniform incident electric fields (i.e., plane waves), and the contribution of surface plasmons to the optical force is best determined with the full MST formalism. On the other hand, the gradient force expression that treats the objects as point dipoles is very useful under the circumstances when it is valid, such as in optical tweezers.

Optical forces between particle dimers have been investigated by a variety of analytical and numerical methods. Numerical investigations of laser-induced forces between interacting nanoscale systems include metallic[19−25] and dielectric[26,27] nanospheres, arrays of metallic nanoparticles,[28] and nanowires.[29,30] The particular case of a plane wave interacting with two 30-nm-radius Ag and Au spheres has been studied by several groups.[19−25] In these studies, the interparticle separation ranged from 0.1 to 1000 nm. Ng et al. have noted some significant quantitative discrepancies among these publications owing to the use of the quasistatic approximation in some cases,[25] but many useful qualitative insights have nonetheless resulted. These include the following: (i) For a given interparticle separation, the wavelength-dependent forces exhibit resonances similar to those for the near-field electromagnetic intensities. The interparticle separation can thus be tuned so that the plasmon resonance of the dimer matches the incident light frequency, producing an enhancement of the light-induced force. (ii) For excitation perpendicular to the interparticle symmetry axis, the optical force is attractive for small particle separations and repulsive for larger particle separations. (iii) For light polarization parallel to the interparticle axis, the optical force is attractive for all interparticle separations studied in the case of Au dimers, whereas attractive and repulsive forces are observed for Ag dimers.[22−25]

The strongest field enhancements and forces arise from structures having sharp features, such as bipyramids and nanorods.[31,32] Such anisotropic metal nanoparticles are especially promising systems for optical studies because their spectra are easily tuned by varying the aspect ratio.[32] In addition, significant field enhancements have been calculated for bipyramids with dimensions readily realized experimentally.[31] Recently, we have developed the plasmon-resonance-based optical trapping (PReBOT) method, a new approach to manipulate single and a few nanoparticles.[15] In PReBOT, the large polarizability associated with the longitudinal plasmon mode of metal nanoparticles is used to enhance the gradient forces of the optical trap. More specifically, stable trapping of Au nanorods and Au bipyramids was demonstrated by detuning the trapping laser to the red side of the plasmon resonance. Two-photon fluorescence measurements indicated stable trapping of single and multiple Au bipyramid nanoparticles and provided insights into interparticle interactions.[16]

In this paper, we determine the interaction between pairs of Au bipyramidal nanoparticles by (i) numerically solving Maxwell's equations using the finite-difference time-domain (FDTD) method,[33] and (ii) compare these results to measured linear scattering spectra of single or multiple trapped nanoparticles. The FDTD method is well-suited for the study of optical properties of complex-shaped metal nanoparticles, such as bipyramids, for which analytical solutions are not currently available. Optical scattering spectra and near-field enhancements are calculated for pairs of Au bipyramids arranged in side-by-side, head-to-tail, and face-on configurations (see Figure 1). The total fields obtained from FDTD are used to calculate optical forces using the Maxwell stress tensor formalism.[13] In addition, the PReBOT method[15] is used to measure scattering spectra of trapped particle(s) for qualitative comparison with the present simulations.

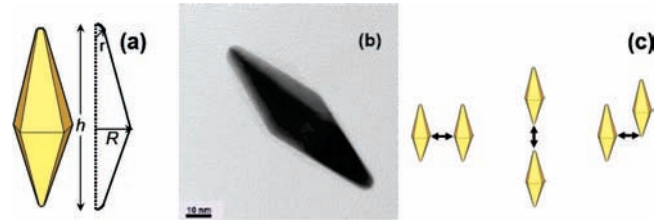

Figure 1. System geometry for the study of plasmonic interactions between Au bipyramids. (a) 3D model of the pentagonal Au bipyramid, with radius $R = 15$ nm, length $h = 83.4$ nm, and tip radius $r = 3.0$ nm. (b) TEM image of a Au bipyramid. (c) Configurations studied: side-by-side (left), head-to-tail (center), and face-on (right). The gap between the particles is indicated by double-sided arrows.

2. Materials and Methods

2.1. Finite-Difference Time-Domain (FDTD) Method. We conducted full-dimensional FDTD calculations;[33] that is, numerically solving Maxwell's equations on 3-D spatial grids. These simulations give the time-dependent electric and magnetic field vectors, $\mathbf{E}(x, y, z, t)$ and $\mathbf{H}(x, y, z, t)$, that result when Au bipyramid nanoparticles are exposed to light. A total field/scattered field approach is used to inject incident waves into the system, and uniaxial perfectly matched layers are used to absorb outgoing waves.[33] An auxiliary differential equation (ADE) approach[34] is used to describe the dispersive and lossy Au dielectric behavior. The ADEs used are equivalent to taking frequency-dependent dielectric function for Au, $\varepsilon_{Au}(\omega)$, to be the sum of a Drude term and three Lorentzian terms, with the corresponding parameters obtained from a fit to experimental data as described in ref 31.

The Au bipyramid was described by a radius at the equator of $R = 15$ nm, total length $h = 83.4$ nm, and radius at the poles of $r = 3$ nm (Figure 1). The surrounding medium is assumed to be water with refractive index $n = 1.33$, or dielectric constant $\varepsilon = n^2 = 1.77$. Unless stated otherwise, the numerical grid spacing was 1 nm and had a time step consistent with the Courant stability criterion.[33]

A variety of FDTD calculations were performed. In the calculations performed to obtain the optical cross sections, the incident wave was taken to be a pulsed sinusoid with polarization along the long axis of the bipyramids (z-axis in our system) and moving normal to the polarization axis (left to right along the x-axis in our system). The pulse was designed to have a frequency content in the range of interest; the $\mathbf{E}(t)$ and $\mathbf{H}(t)$ fields on the sides of a 3-D box surrounding the nanoparticles are Fourier transformed into frequency space and saved. Subsequent calculations of surface integrals over the frequency-resolved Poynting vector yield the optical cross sections.[35] We generally carried out separate calculations to obtain full-field profiles and field enhancements at particular wavelengths of interest. For these calculations, we used a continuous wave source at the appropriate frequency. The optical force calculations were more involved, and the next subsection discusses their determination.

2.2. Optical Force. Our system consists of two metal nanoparticles in a dielectric medium. The time-averaged force on one of the nanoparticles is (SI units),[36]

$$\langle \mathbf{F} \rangle = \int_V \langle \rho \mathbf{E} + \mathbf{J} \times \mathbf{B} \rangle \, dV \qquad (1)$$

where V is any volume that contains only the nanoparticle in question; ρ is the electric charge density; $\mathbf{J}$ is the current density; and $\mathbf{B} = \mu\mu_0\mathbf{H}$, where μ is the medium magnetic permeability, μ_0 is the magnetic constant, and $\mathbf{H}$ is the magnetic field. Note that V can be any volume encompassing the nanoparticle that does not include the other one because ρ and $\mathbf{J}$ are zero in the dielectric medium (true for the interparticle separations studied here). The angular brackets indicate a time average (i.e., averaged over an optical cycle). The term $\rho\mathbf{E} + \mathbf{J} \times \mathbf{B}$ is simply the continuum limit force per unit volume that is analogous to the Lorentz force law for the force acting on a moving, charged particle in the presence of an electromagnetic field. Although eq 1 is the most intuitive and correct form for the optical force, a more computationally convenient form involves replacing the volume integral with a surface integral (eq 3, below).

Equation 1 is difficult to evaluate in numerical calculations based on grids because it is dominated by surface terms. With some effort,[36] it is possible to show that $\langle\rho\mathbf{E} + \mathbf{J} \times \mathbf{B}\rangle$ in the integrand of eq 1 can be replaced with $\langle\nabla\cdot\overleftrightarrow{\mathbf{T}}\rangle$, where Maxwell's stress tensor, $\overleftrightarrow{\mathbf{T}}$, is

$$\overleftrightarrow{\mathbf{T}} = \varepsilon\varepsilon_0\mathbf{EE} + \mu\mu_0\mathbf{HH} - \frac{1}{2}(\varepsilon\varepsilon_0|\mathbf{E}|^2 + \mu\mu_0|\mathbf{H}|^2) \quad (2)$$

where ε_0 is the free-space permittivity. Application of Gauss' law then leads to the surface integral,

$$\langle\mathbf{F}\rangle = \int_S \langle\overleftrightarrow{\mathbf{T}}\rangle\cdot\mathbf{n}\,\mathrm{da} \quad (3)$$

where S is any arbitrary surface containing only the nanoparticle, $\mathbf{n}$ is the unit normal vector to this surface, and da is a differential element of surface area.

Equations 13 concern time averages over the real-valued electric and magnetic fields, $\mathbf{E}(x, y, z, t)$ and $\mathbf{H}(x, y, z, t)$. We are generally interested in evaluating $\langle\mathbf{F}\rangle$ at a specific frequency, ω. In our FDTD calculations, this can be accomplished with the use of a continuous wave (CW) source, which drives the system into a sinusoidal steady state; that is, one with only $\cos(\omega t)$ and $\sin(\omega t)$ dependence. The explicit time averages can then be evaluated "on the fly" during the FDTD calculation. An alternative to the explicit time average is to calculate the complex-valued phasor analogs of $\mathbf{E}(t)$ and $\mathbf{H}(t)$, denoted by $\mathbf{E}_c(\omega)$ and $\mathbf{H}_c(\omega)$. We infer the phasors via Fourier transformation of the fields from time, t, to frequency, ω. (See the Appendix for a brief discussion of some subtle points concerning the correct determination of the phasors.) The phasors can be generated from the FDTD calculations and saved after the calculation for more facile postprocessing. One can then conveniently examine the MST or its components, or other functions of $\mathbf{E}$ and $\mathbf{H}$, with relative ease. The time-averaged $\langle\overleftrightarrow{\mathbf{T}}\rangle$ entering in eq 3, using phasors, is

$$\langle\overleftrightarrow{\mathbf{T}}\rangle = \frac{1}{2}\left[Re\left(\varepsilon\varepsilon_0\mathbf{E}_c\mathbf{E}_c^* + \mu\mu_0\mathbf{H}_c\mathbf{H}_c^*\right) - \frac{\overleftrightarrow{\mathbf{I}}}{2}\left(\varepsilon\varepsilon_0|\mathbf{E}_c|^2 + \mu\mu_0|\mathbf{H}_c|^2\right)\right] \quad (4)$$

where $\mathbf{E}_c\mathbf{E}_c^*$ and $\mathbf{H}_c\mathbf{H}_c^*$ are tensor outer products, and $\overleftrightarrow{\mathbf{I}}$ is the identity tensor.

Equations 3 and 4 were used to evaluate the force with the surface of integration being over a box enclosing one of the bipyramids. Finally, an optical intensity of $I_0 = 5$ MW/cm^2 was used in the force calculations. We assumed that $I_0 = \langle\mathbf{E}_0 \times \mathbf{H}_0\rangle = c\varepsilon_0 n E_0^2/2$, the relation between I_0 and the maximum amplitude, E_0, of the real-valued incident field, holds. Here, n is the refractive index of the medium [e.g., typically, our incident wave is a plane wave, $\mathbf{E}_0(t) = \hat{z}\,E_0\cos(n\omega x/c - \omega t)$].

2.3. Linear-Scattering Measurements of Au Bipyramids Trapped with PReBOT.[15,16] The Au bipyramids were optically trapped using a tunable home-built continuous-wave Ti:Sapphire oscillator operating at 820 nm. Au bipyramids with a longitudinal plasmon (peak) resonance wavelength of 800 nm were synthesized according to literature protocols.[32] The Au bipyramids were stabilized with an aqueous solution of CTAB (cetyltrimethylammonium bromide; low mM concentration). The solution was cooled to 4 °C, causing the CTAB to precipitate out. The supernatant was subsequently removed and diluted for use in the PReBOT trapping measurements. The CW trapping laser was expanded to overfill the back aperture of an Olympus UPLSAPO 60X water-immersion objective lens. The laser power at the focus was estimated to be 40 mW on the basis of the manufacturer's specifications. In addition, a home-built femtosecond (10 fs pulse; > 180 nm bandwidth) Ti:Sapphire oscillator was used as a scattering light source, and its power was kept to ≪10 mW. A time series of scattering spectra was recorded with a 100 ms integration time on an Ocean Optics SD1000 fiber-coupled spectrometer.

3. Results and Discussion

3.1. Optical Spectra of Au Bipyramidal Dimers in Different Configurations. The calculated scattering spectra of Au bipyramidal dimers change as a function of interparticle gap, d, as shown in Figure 2. The plasmon spectrum for particles in the side-by-side configuration blue-shifts with decreasing separation (second panel); from 818 nm at $d = \infty$ nm separation to 807 nm at $d = 16$ nm separation to 789 nm at $d = 2$ nm. The same spectral shifts are obtained for another side-by-side configuration in which the interparticle axis is orthogonal to the wave-vector direction of the incident radiation and both particles directly face the incident field (i.e., 90° rotated geometry; not shown). In contrast, spectra for both face-on and head-to-tail configurations exhibit a large red shift of the peak wavelength as the gap decreases: the peak shifts by 50 and 105 nm for the face-on and head-to-tail cases for $d = 2$ nm, respectively (Figure 2, first and third panels). Therefore, a relatively small range of interparticle separations gives a wide range of contrasting behaviors in the optical response of the Au bipyramidal dimers.

The relationship between interparticle plasmon coupling and the scattering spectra versus interparticle separation can be qualitatively described using a model based on dipole−dipole interactions.[37,38] Recently, this model has been used to describe a universal scaling behavior of spectral shifts vs interparticle separation for a range of nanoparticle sizes, shapes, orientations, metal types, and dielectric constants of the surrounding medium. This model is the basis for the so-called "plasmon-ruler" equation that uses the universal scaling behavior mentioned above to model spectral shifts of coupled metal nanoparticles.[38] Figure 2 (bottom panel) shows a plot of the plasmon shift, $\Delta\lambda$, versus interparticle separation after scaling the shift and separation by the single-particle plasmon wavelength maximum, λ_0, and particle size, D, respectively. Following the dipole-coupling model, D is the particle dimension along the interparticle interaction axis. From Figure 1a, $D = d + 2R$ for side-by-side and face-on configurations, and $D = d + h$ for the head-to-tail

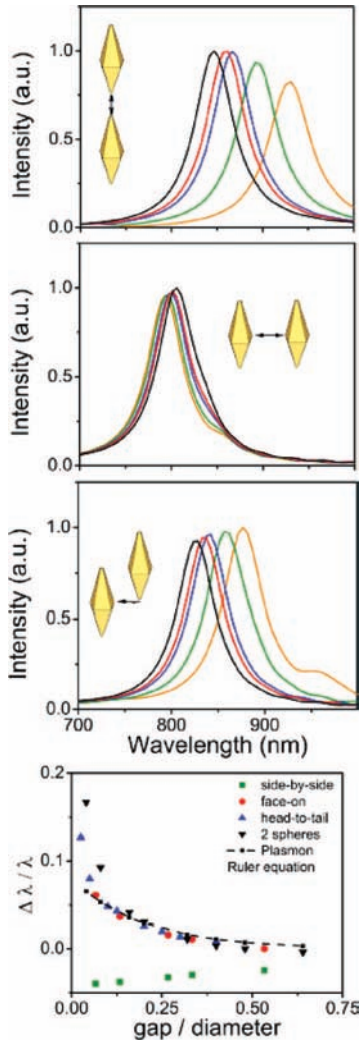

Figure 2. Scattering spectra as a function of separation for bipyramid Au nanoparticle dimers in head-to-tail (top), side-by-side (second panel), and face-on (third panel) configurations. Gap (nm): 2 (orange line); 4 (green); 8 (blue); 10 (red); 16 (black). Bottom panel: Fractional plasmon shift versus gap/diameter ratio for the three different configurations and for two Au spheres with 50 nm diameter.

geometry. Figure 2 (bottom panel) shows that the Au bipyramids in face-on and head-to-tail configurations have almost identical scaled behavior at all separations studied. Their behavior is qualitatively similar to that obtained from the plasmon-ruler equation (dashed line).

Also included in Figure 2 (bottom panel) are the corresponding results for a pair of Au nanospheres of 50 nm diameter, which have the same volume as the Au bipyramids. In the simulations, the symmetry axis of the Au nanosphere dimer is parallel to the polarization of the incident field. At large separations, for a gap/diameter range between 0.2 and 0.6, there is good agreement between the results for bipyramidal (face-on and head-to-tail configurations) and spherical particles. At short interparticle spacings, the quantity $\Delta\lambda/\lambda$ is found to be larger for spheres than for bipyramids. This is due to the D scaling factor: the near-field intensity between resonantly excited bipyramids extends over much longer distances when compared to that of spheres having the same volume.[31]

3.2. Near-Field Intensity Enhancement. The near-field intensity enhancement associated with excitation of the (coupled) plasmon of Au bipyramid dimers was calculated as a function of separation for side-by-side, head-to-tail, and face-on configurations. The normalized intensity enhancement is $\langle \mathbf{E}^2 \rangle / \langle \mathbf{E}_0^2 \rangle = Re|\mathbf{E}_c|^2/\mathrm{Re}|\mathbf{E}_{0c}|^2$, where $\mathbf{E}_c$ is the Fourier transform of the time-evolving field (see the Appendix). For all three configurations, the separations explored were 2, 4, 8, 10, 16, 20, 24, and 32 nm. We calculated field enhancements at the plasmon resonance for each gap to quantify the largest enhancement factor from a pair of Au bipyramidal nanoparticles (see Table 1).

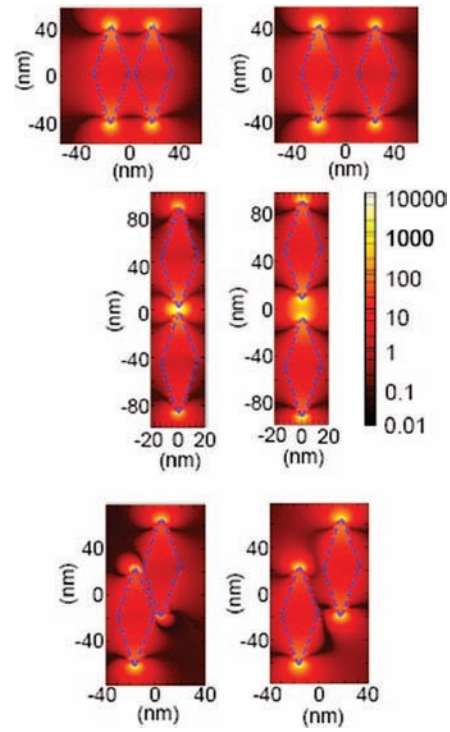

Figure 3. Field enhancement for a pair of Au bipyramids in side-by-side (top), head-to-tail (center), and face-on (bottom) configurations. Left column, 4 nm gap; right column, 16 nm gap. Each bipyramid is described by $R = 15$ nm, $h = 83.4$ nm, and $r = 3$ nm. The grid size for the FDTD calculations is 1 nm. In both cases, the incident field polarization is parallel to the interparticle axis. The incident wavelength matches the plasmon resonance at each separation for all three configurations. The boundary between the nanoparticle and the medium is marked by blue dashed lines.

TABLE 1: Intensity Enhancement Factors for Two Au Bipyramids[a]

	I/I_0	
geometry and separation (nm)	$d = 4$	$d = 16$
side-by-side	1200	2500
face-on	3000	2500
head-to-tail	10000	3500

[a] The incident wavelength matches the plasmon resonance of the dimer for each geometry and for each inter-particle separation.

The intensity distributions calculated with FDTD are shown in Figure 3. As in the case of a single Au bipyramidal nanoparticle, the largest local field enhancement factors are observed near the tips.[31] The enhancements for the dimers are not the sum of the enhancements from each particle, which would be expected for noninteracting systems. Instead, the field on each particle is the combination of the incident field, the particle polarization response, and the field due to interaction with the nearby particle. In the case of two coupled metal nanoparticles, the total electric field is determined self-consistently either analytically or by numerical methods. The present results show that the range of separations studied leads to contrasting near-field responses for different configurations.

Side-by-Side Configuration. The intensity enhancement factors in the side-by-side geometry are shown in Figure 3 (top row) for separations equal to 4 (left) and 16 nm (right). For each separation, the spatial intensity distributions around each particle exhibit a dipole-like pattern, with the largest enhancement near the tips. The largest enhancement factor decreases monotonically as the separation between particles decreases (from $I/I_0 = 1000$ at 2 nm to 2500 at 32 nm). The gap-dependence of the scattering spectra of side-by-side dimers (Figure 2) shows a blue shift of the plasmon resonance with decreasing gap relative to the plasmon resonance of the single particle, $\lambda = 818$ nm. These results indicate weak plasmonic interaction between particles in the side-by-side configuration, consistent with the far-field spectra shown in Figure 2.

The intensity enhancement factor is larger, by a factor of 2, for the particle that interacts first with the incident field (i.e., the field enters from the left in Figure 3). As a result, the sum of the largest enhancement factors for the two bipyramids is less than twice the enhancement factor for a single bipyramid. The smaller intensity enhancement for the particle farther from the incident field is due to scattering and absorption of light by the first particle. In contrast, the same intensity enhancement is obtained for both particles in another possible side-by-side configuration, in which the interparticle axis is orthogonal to the wave-vector direction.

Head-to-Tail Configuration. The intensity enhancement factors in the head-to-tail configuration are shown in Figure 3 (center row) for separations equal to 4 (left) and 16 nm (right). A monotonically decreasing enhancement factor was observed with increasing interparticle separation. A field enhancement factor $|E|/|E_0|$ of 500 was obtained for the 2 nm gap using an incident wavelength of 931 nm, which matches the plasmon resonance wavelength at this separation. The large values of $|E|/|E_0|$ are the field enhancements at the tips of the bipyramid and contain a contribution from the enhanced local field of the second particle that interacts with the first particle. As shown previously, the maximum field enhancement is related to the curvature of the tip,[31] and sharper tips can lead to even higher enhancements.

Face-On Configuration. The intensity enhancement factors in the face-on configuration are shown in Figure 3 (bottom row) for separations equal to 4 (left) and 16 nm (right). The normalized intensities around each particle show a dipole-like pattern, as in the side-by-side configuration.

3.3. Optical Forces between Au Bipyramids. The optical forces between Au bipyramids are calculated as outlined in Section 2.2. We find that magnetic and off-diagonal terms, where $i \neq j$ in eq 4, make a negligible contribution to the optical force calculated using eq 3. For completeness, however, the calculated forces include all terms and components of the MST in eq 4. We validated our rigorous FDTD-based optical force approach by carrying out calculations on a system consisting of two Ag spheres of 60 nm diameter for which there are previous, rigorous electrodynamics results to compare with.[25] For example, the optical force was found to be 55 pN at 6 nm separation, whereas Figure 3 in ref 25 indicates a force of $\approx$60 pN. We note, however, that significant differences in the force calculated from rigorous electrodynamics methods and approximate (quasistatic) analytical methods were found at separations of less than 10 nm, as indicated previously.[19−25] In the following, the MST calculations of the optical force are examined with a focus on the interaction between Au bipyramids in side-by-side and head-to-tail configurations.

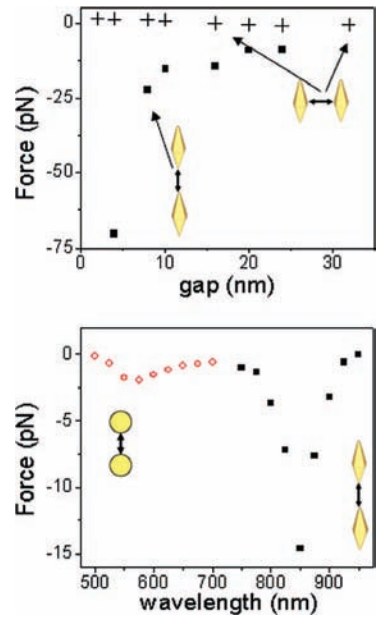

Figure 4. FDTD simulation Maxwell stress tensor analysis of forces between pairs of Au nanoparticles. Top: two bipyramids in head-to-tail (squares) and side-by-side (crosses) configurations for various distances. The input wavelength was chosen to match the plasmon resonance of the dimer at each separation. (bottom) Wavelength dependence of the optical force at a constant separation of 16 nm: two spheres (circles) and two bipyramids in head-to-tail configuration (squares). In both cases, the incident field polarization is parallel to the interparticle axis. Intensity: 5 MW/cm^2.

Figure 4 (top) shows the calculated optical force as a function of separation for the head-to-tail and side-by-side configurations. The range of separations studied is from 4 to 32 nm, and in each case, the wavelength of the incident fields is chosen to match the plasmon resonance of the dimer (see Figure 2). At short range, the optical force rises very rapidly in the head-to-tail configuration as the interparticle separation decreases. This trend reflects strong interparticle interactions at short separations, as already inferred from the spatial intensity profiles (see Figure 3). A weak repulsive force is observed for the side-by-side configuration, consistent with the gap-dependence of the scattering spectra for the same geometry (see Figure 2).

The wavelength dependence of the optically induced forces at a constant interparticle gap of 16 nm is shown in Figure 4 (bottom) for a pair of Au bipyramids and a pair of Au spheres. The optical forces in the head-to-tail geometry at 16 nm interparticle separation are a factor of 4 stronger than the force calculated for a pair of spherical nanoparticles with the same volume as the bipyramids (i.e., 25 nm radius). In both cases, the optical force exhibits a resonance and is always attractive for polarization parallel to the interparticle axis. The force peaks near the surface plasmon resonance of the dimer at each separation (see Figure 2), thus following the same trend observed for the field enhancement factor (see Figure 3).

The combined MST/FDTD approach to the calculation of optical forces provides insights into plasmonic interactions between Au bipyramidal nanoparticle dimers in different geometries. We observe that both significant attraction and weak repulsion can be obtained depending on the relative arrangement of the particles. Moreover, for polarization parallel to the interparticle axis, the spectra of optical forces are attractive and exhibit an absorptive line shape in the range of interparticle separations studied.

The results shown in Figure 4 suggest that plasmonic forces between two Au bipyramids are qualitatively different from the

gradient force obtained within the dipole approximation. Gradient forces can be either attractive or repulsive, exhibiting a maximum force on the red side of the dipolar plasmon mode (resonance).[10] Furthermore, these forces are proportional to the real part of the polarizability multiplied by the intensity gradient of the incident optical beam:[10]

$$\langle F \rangle = \frac{1}{4} Re[\alpha] \frac{\partial |E|^2}{\partial x} \quad (5)$$

where α is the single-particle polarizability and E is the amplitude of the incident field.

In contrast, we use an incident plane wave in our calculations, and the resulting intensity gradient associated with the incident beam is therefore zero. The inhomogeneous field distributions that give rise to the optical forces between two Au bipyramids have two origins: the resonant field enhancement around each particle and interparticle plasmonic coupling. In addition, given the large absorption and scattering cross sections of metallic nanoparticles near resonance, plasmon-induced forces are sensitive to both absorptive and dispersive features of the dimer polarizability, whereas eq 5, above, predicts that the wavelength dependence of the gradient force is given solely by the dispersive component.

A more general expression for the average total optical force on a small particle due to an arbitrary electric field distribution, based on the coupled-dipole approximation (CDA), has been derived recently. For two interacting metal nanoparticles in the presence of a plane wave with polarization parallel to the interparticle axis, the time-averaged force on a single particle along the direction of the interparticle axis is then approximated by[39,40]

$$\langle F_{1z} \rangle = \frac{1}{4} Re[\alpha] \frac{\partial |E_{1z}|^2}{\partial z} - \frac{1}{2} \mathrm{Im}[\alpha] \, \mathrm{Im}\left[E_{1z} \frac{\partial E_{1z}^*}{\partial z} \right] \quad (6)$$

where the asterisk, *, denotes the complex conjugate. This formula reduces to the gradient force when the electric field is real, as in the case of beams commonly employed in optical tweezers. In addition, it establishes the importance of (i) the spatial dependence of the field, (ii) the radiative reaction term in the particle polarizability, and (iii) higher-order corrections to the dipole approximation.[40] The CDA method, originally introduced to study the scattering of light by nonspherical dielectric grains in free space,[41] has been recently applied to the determination of electromagnetic forces between plasmonic particles[40] and of forces on nanoparticles over flat dielectric substrates.[42,43] We find the discussion of ref 40 to be particularly clear and useful and have implemented their eq 3 (eq 6, above).

We performed coupled-dipole approximation (CDA) calculations to investigate the physical mechanisms that contribute to the observed wavelength dependence of the optical forces. These physically intuitive results complement our findings from the FDTD calculations. Our findings for a pair of 5-nm-radius Ag spheres are consistent with recent analytical and numerical studies of optical forces between spherical metal nanoparticles.[21−25,40] The results of CDA calculations for a pair of 25-nm-radius Au spheres with an interparticle gap of 16 nm, shown in Figure 5 (bottom), are in close agreement with the FDTD results for the same system (Figure 4). An absorptive line shape is also observed for separations from 1 to 5 nm (Figure 5, top). Interestingly, a similar calculation for a pair of 25-nm-radius Ag spheres yields a dispersive line shape in which the force is

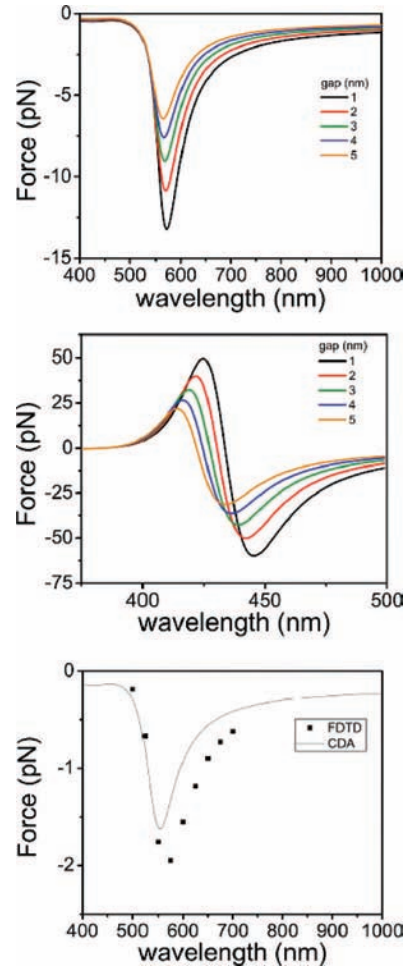

Figure 5. Spectra of the optical force between pairs of spherical metal nanoparticles as a function of interparticle separation, using the coupled-dipole approximation. (top) Au; (center) Ag. The bottom panel shows the optical force between two Au particles at 16 nm separation from FDTD (solid squares) and CDA (solid line). The polarization of the incident field is parallel to the interparticle axis. Particle radius: 25 nm. Intensity: 5 MW/cm^2.

transformed from repulsive to attractive with increasing wavelength of the incident field. Figure 5 (center) shows that the maximum forces are nearly 4 times larger than the forces calculated for Au. Therefore, we observe that both absorptive and dispersive force lineshapes can be obtained for a given system geometry, depending on the metal nanoparticle composition. These results suggest that it would be more difficult to trap single Au nanoparticles, as compared to Ag. On the other hand, the trap stability is expected to be more sensitive to interparticle separation fluctuations in the case of Ag, where a dispersive line shape is obtained. Figure 6 shows a line shape analysis of the optical forces. The force spectra are largely absorptive for a pair of Au bipyramids with interparticle separations ranging from 2 to 24 nm, and a small dispersive feature (~3% weight) is observed. Although we have not attempted to directly fit a fundamental equation to the data, the results of Figure 5 (bottom) and Figure 6 are almost mirror images. This is a surprising result whose origin is under further investigation. The opposite line shape asymmetries might result from (i) a retardance effect for the nearly 200 nm end-to-end distance or (ii) a change in the effective wavelength-dependent polarizability associated with the coupled-particle resonance. We will also consider the effect of the strong electric fields that occur at the tips of the bipyramids (internal and external to the

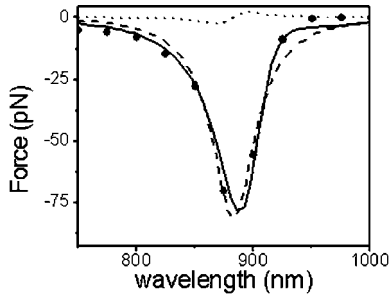

Figure 6. Fit of the spectrum of optical forces for a pair of Au bipyramids at $d = 4$ nm to a Lorentzian and its derivative. Open circles: force calculated from MST analysis of the FDTD data. Solid line: line shape fitting. Dashed line: Lorentzian fit. Dotted line: derivative of the Lorentzian fit. The incident field polarization is parallel to the interparticle axis. Intensity: 5 MW/cm^2.

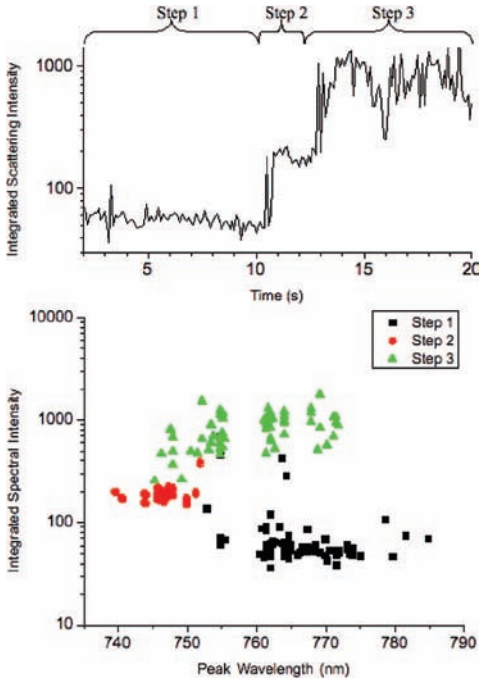

Figure 7. Experimental nanoparticle trapping of Au bipyramids with the PReBOT setup. (top) Time trajectory of the integrated scattering intensity acquired with a 100 ms integration time; (bottom) peak scattering wavelength analysis of the time-trajectory shown at the top. The time trace of the wavelength-integrated scattering intensity (top) shows the sequential loading of Au bipyramids. The labels "Step 1", "Step 2", and "Step 3" indicate signal level changes that occur as 1, 2, and 3 particles are loaded into the trap, respectively. Stable trapping of one and two particles is observed, whereas there is an apparent instability for three particles in the trap. The bottom figure shows a spectral blue shift of the scattered light as the second particle enters the trap.

particles) as a result of plasmon excitation and their effect on altering the dynamics of the electrons in those regions that could, in turn, affect the polarizability and observed line shape.

3.4. Connection with Experimental Results. A time-trajectory of the wavelength-integrated scattered intensity recorded by a CCD array detector as a function of time is shown in Figure 7 (top). This trajectory shows the successive entry of 1, 2, and 3 particles into the optical trap, labeled step 1, 2 and 3. Figure 7 (bottom) shows the corresponding peak scattering wavelength, taken from the unnormalized spectral traces (i.e., the peak wavelength are not corrected for the finite, ~180 nm, bandwidth of the femtosecond pulsed source used for detection).

The data show that the addition of a second particle into the optical trap produces a clear blue shift in the observed scattering spectrum. These data imply that the particles in the trap are adopting the side-by-side configuration, as this is the only geometry (from our calculations) that produces blue shifts in the collective plasmon resonance of the two particles. Face-on and head-to-tail geometries would result in a red shift of the plasmon resonance and actually destabilizing the particles in the optical trap. Determination of the time-evolving scattering spectra for multiply trapped Au bipyramids is the subject of ongoing work.

4. Conclusions

We have presented a numerical study of the near- and far-field optical properties of pairs of bipyramidal Au nanoparticles in different arrangements: head-to-tail, side-by-side, and face-on. A red shift of the plasmon resonance is calculated when two particles approach each other in either head-to-tail or face-on geometry, whereas a small blue shift occurs for the side-by-side configuration. For these three geometries, the spectral shifts at various interparticle separations are consistent with scaling predictions of a simple dipole-coupling model. The normalized near-field spatial intensity distributions are consistent with a dipolar plasmon resonance for side-by-side and face-on configurations as well as for the head-to-tail geometry at long interparticle separations. Furthermore, a strong field enhancement is observed at the gap between particles in the head-to-tail arrangement for small separations. The maximum field enhancements are observed when the incident field wavelength matches the plasmon resonance of the dimer.

We used the Maxwell stress tensor formalism to calculate optical forces between nanoparticles. We find that the optical force can be either attractive or repulsive, depending on the arrangement of the particles. At a fixed separation and for light polarization parallel to the interparticle axis, the force exhibits an absorptive line shape as the incident wavelength is varied through the surface plasmon resonance of the dimer, thereby indicating the importance of the imaginary part of the dielectric constant of Au for plasmonic trapping. When this part dominates, the force spectrum is quite different from that which would be expected upon consideration of the gradient force formula. In addition, the force in the head-to-tail configuration is over 2 orders of magnitude larger than the force in the side-by-side geometry, and an order of magnitude larger than the corresponding force between two spherical Au nanoparticles with the same volume as the bipyramids. The simulation results for the side-by-side geometry are qualitatively consistent with experimental results; that is, the two-particle scattering spectrum is more intense and blue-shifted compared to that for single particles (Au bipyramids).

The coupled-dipole approximation of refs 39 and 40 was particularly useful in interpreting the qualitative features of our rigorously calculated MST/FDTD forces. Finally, our results imply that strong plasmonic forces and optical trapping could be achieved from engineering dimers (or possibly trimers, etc.) of bipyramidal particles in the head-to-tail configuration.

Appendix

Phasor Conventions. Our FDTD calculations lead to the real-valued electric and magnetic field vectors as a function of time, $\mathbf{E}(t)$ and $\mathbf{H}(t)$, suppressing the spatial dependence of the vectors. Suppose we have driven the system into a sinusoidal steady-state via application of a continuous wave source. If $\mathbf{F}(t)$ denotes such a sinusoidal steady-state vector, its time-dependence is of the form

$$\mathbf{F}(t) = \mathbf{A}\cos(\omega t) + \mathbf{B}\sin(\omega t) \quad \text{(A1)}$$

Its frequency-domain, complex phasor analog, $\mathbf{F}_c(\omega)$, is defined to be such that

$$\mathbf{F}(t) = Re[\mathbf{F}_c(\omega)\exp(-i\omega t)] \quad \text{(A2)}$$

If T is some time such that (A1) is valid, then it is straightforward to see from A1 and A2 that

$$\mathbf{F}_c(\omega) = \frac{2}{\tau}\int_T^{T+\tau}\mathbf{F}(t)\exp(\omega t)\,dt \quad \text{(A3)}$$

where $T = 2\pi/\omega$, and it is important to note the factor of 2 in the prefactor of the integral. The time-average of $\mathbf{F}^2 \equiv \mathbf{F}\cdot\mathbf{F}$ is then related to $\mathbf{F}_c$ according to

$$\langle\mathbf{F}^2\rangle \equiv \frac{1}{\tau}\int_T^{T+\tau}\mathbf{F}\cdot\mathbf{F}\,dt = \frac{1}{2}[\mathbf{F}_c\cdot\mathbf{F}_c^*] \quad \text{(A4)}$$

and more generally, one can show that the time-average of a tensor outer product $\mathbf{FG}$ is

$$\langle\mathbf{FG}\rangle \equiv \frac{1}{\tau}\int_T^{T+\tau}\mathbf{FG}\,dt = \frac{1}{2}\mathrm{Re}[\mathbf{F}_c\mathbf{G}_c^*] \quad \text{(A5)}$$

Acknowledgment. We thank Gary Wiederrecht for insightful conversations, Tom Spears for his role in building the femtosecond laser system, and Tae-Woo Lee and Mingzhao Liu for assistance with the FDTD calculations. Work at Argonne National Laboratory was supported by the U.S. Department of Energy, Office of Science, Offices of Basic Energy Sciences, under Contract No. DE-AC02-06CH11357. NFS was supported by the National Science Foundation (CHE-0317009).

References and Notes

(1) Parthasarathy, R.; Lin, X.-M.; Elteto, K.; Rosenbaum, T. F.; Jaeger, H. M. *Phys. Rev. Lett.* **2004**, *92*, 076801.
(2) Bigioni, T. P.; Lin, X.-M.; Nguyen, T. T.; Corwin, E.; Witten, T. A.; Jaeger, H. M. *Nat. Mater.* **2006**, *5*, 265–270.
(3) Raether, H. *Surface Plasmons*; Springer Tracts in Modern Physics; Springer: Berlin, 1988; Vol. 111.
(4) Rechberger, W.; Hohenau, A.; Leitner, A.; Krenn, J. R.; Lamprecht, B.; Aussenegg, F. R. *Opt. Commun.* **2003**, *220*, 137–141.
(5) Kelly, K. L; Coronado, E.; Zhao, L. L.; Schatz, G. C. *J. Phys. Chem. B* **2003**, *107*, 668–677.
(6) Romero, I.; Aizpurua, J.; Bryant, G. W.; Garcia de Abajo, F. J. *Opt. Express* **2006**, *14*, 9988–9999.
(7) Xu, H.; Käll, M. *Phys. Rev. Lett.* **2002**, *89*, 246802.
(8) Collier, C. P.; Saykally, R. J.; Shiang, J. J.; Henrichs, S. E.; Heath, J. R. *Science* **1997**, *277*, 1978–1981.
(9) Atay, T.; Song, J. H.; Nurmikko, A. V. *Nano Lett.* **2004**, *4*, 1627–1631.
(10) Ashkin, A.; Dziedzic, J. M.; Bjorkholm, J.; Chu, S. *Opt. Lett.* **1986**, *11*, 28–90.
(11) Novotny, L.; Bian, R. X.; Xie, X. S. *Phys. Rev. Lett.* **1997**, *79*, 645–648.
(12) Okamoto, K.; Kawata, S. *Phys. Rev. Lett.* **1999**, *83*, 4534–4537.
(13) Chaumet, P. C.; Rahmani, A.; Nieto-Vesperinas, M. *Phys. Rev. Lett.* **2002**, *88*, 123601.
(14) Quidant, R.; Petrov, D.; Badenes, G. *Opt. Lett.* **2005**, *30*, 1009.
(15) Pelton, M.; Liu, M.; Kim, H.-Y.; Smith, G.; Guyot-Sionnest, P.; Scherer, N. F. *Opt. Lett.* **2006**, *31*, 2075–2077.
(16) Toussaint, K. C., Jr.; Liu, M.; Pelton, M.; Pesic, J.; Guffey, M. J.; Guyot-Sionnest, P.; Scherer, N. F. *Opt. Express* **2007**, *15*, 12017–12029.
(17) Yannopapas, V. *Phys. Rev. B* **2008**, *78*, 045412.
(18) Nieto-Vesperinas, M.; Chaumet, P. C.; Rahmani, A. *Philos. Trans. R. Soc. London* **2004**, *362*, 719–737.
(19) Arias-Gonzalez, J. R.; Nieto-Vesperinas, M. *J. Opt. Soc. Am.* **2003**, *20*, 1201.
(20) Novotny, L.; Henkel, C. *Opt. Lett.* **2008**, *33*, 1029–1031.
(21) Quidant, R.; Zelenina, A. S.; Nieto-Vesperinas, M. *Appl. Phys. A: Mater. Sci. Process.* **2007**, *89*, 233–239.
(22) Hallock, A. J.; Redmond, P. L.; Brus, L. E. *Proc. Natl. Acad. Sci. U.S.A.* **2005**, *102*, 1280.
(23) Chu, P.; Mills, D. L. *Phys. Rev. Lett.* **2007**, *99*, 127401.
(24) Chu, P.; Mills, D. L. *Phys. Rev. B* **2008**, *77*, 045416.
(25) Ng, J.; Tang, R.; Chan, C. T. *Phys. Rev. B* **2008**, *77*, 195407.
(26) Wong, V.; Ratner, M. A. *J. Opt. Soc. Am. B* **2006**, *23*, 1801–1814.
(27) Benito, D. V.; Simpson, S. H.; Hanna, S. *Opt. Express* **2008**, *16*, 2942.
(28) Yannopapas, V. *Phys. Rev. B* **2008**, *78*, 045412.
(29) Haltermann, K.; Merle Elson, J.; Singh, S. *Phys. Rev. B* **2005**, *72*, 075429.
(30) Lamothe, E.; Leveque, G.; Martin, O. J. F. *Opt. Express* **2007**, *15*, 9631–9644.
(31) Liu, M.; Guyot-Sionnest, P.; Lee, T. W.; Gray, S. K. *Phys.Rev. B* **2007**, *76*, 235428.
(32) Liu, M.; Guyot-Sionnest, P. *J. Phys. Chem. B* **2005**, *109*, 22192–22200.
(33) Taflove, A.; Hagness, S. C. Computational Electrodynamics. *The Finite-Difference Time-Domain Method*, 2nd ed.; Artech House: Boston, 2000.
(34) Gray, S. K.; Kupka, T. *Phys. Rev. B* **2003**, *68*, 045145.
(35) Bohren, C. F.; Huffman, D. *Absorption and scattering of light by small particles*, John Wiley: New York, 1983.
(36) Novotny, L.; Hecht, B. *Principles of Nano-Optics*; Cambridge University Press: New York, 2007.
(37) Su, K. H.; Wei, Q.-H; Zhang, X.; Mock, J. J.; Smith, D. R.; Schultz, S. *Nano Lett.* **2003**, *3*, 1087–1090.
(38) Jain, P. K.; Huang, W.; El-Sayed, M. A. *Nano Lett.* **2007**, *7*, 2080–2088.
(39) Chaumet, P. C.; Nieto-Vesperinas, M. *Opt. Lett.* **2000**, *25*, 1065.
(40) Sepulveda, B.; Alegret, J.; Kall, M. *Opt. Express* **2007**, *15*, 14914.
(41) Purcell, E. M.; Pennypacker, C. R. *Astrophys. J.* **1973**, *186*, 705.
(42) Chaumet, P. C.; Rahmani, A.; de Fornel, F.; Dufour, J.-P. *Phys. Rev. B* **1998**, *58*, 2310.
(43) Chaumet, P. C.; Nieto-Vesperinas, M. *Phys. Rev. B* **2000**, *61*, 14119.

JP811068J